IEEE Access
Multidisciplinary ⋮ Rapid Review ⋮ Open Access Journal

Received July 7, 2021, accepted July 20, 2021, date of publication July 26, 2021, date of current version July 30, 2021.

Digital Object Identifier 10.1109/ACCESS.2021.3099946

Battery-Less NFC Bicycle Tire Pressure Sensor Based on a Force-Sensing Resistor

MARTI BOADA, ANTONIO LAZARO, (Senior Member, IEEE), RAMON VILLARINO, ERNEST GIL-DOLCET, AND DAVID GIRBAU, (Senior Member, IEEE)
Department of Electronic, Electric and Automatic Engineering, Universitat Rovira i Virgili, 43007 Tarragona, Spain

Corresponding author: Antonio Lazaro (antonioramon.lazaro@urv.cat)

This work was supported in part by Grant BES-2016-077291, in part by the Spanish Government under Project RTI2018-096019-B-C31, and in part by the European Union's European Regional Development Fund (ERDF).

ABSTRACT This paper describes a novel low-cost tire pressure monitoring system (TPMS) for bicycles. The system is based on a battery-less near field communication (NFC) tag that integrates a pressure sensor, which is placed between the tire and the inner tube. The system uses no battery since the energy is obtained from the magnetic field induced by the reader in order to establish the communication. The pressure can be read by any NFC-enabled reader such as a smartphone. The pressure sensor is a force-sensing resistor (FSR) that controls the oscillation frequency of a 555 timer-based oscillator. The frequency is read and computed by a microcontroller, and the result is written via I^2C bus to the memory of a near-field communication integrated circuit (IC), which is read by a commercial smartphone or NFC reader. A prototype is designed on an FR4 substrate which integrates a 12×16 mm antenna connected to the NFC IC (NT3H211 from NXP). The proposed prototype has a 3D-printed enclosure to protect the components mounted on the surface of the PCB and to protect the tire from punctures. A system for characterizing the read range is presented. The tag requires a minimum magnetic field of 2.9 A_{RMS}/m to operate up to a distance of 8 mm between reader and the tire, providing enough power to supply energy to the whole circuitry and to receive the information stored at the NFC IC. The system has been tested with a 59 mm-width mountain bike tire. The sensor has been characterized using a simple polynomial fitting to obtain the pressure from the measurement of the oscillation frequency. An accuracy of 0.1 has been accomplished in the range of 0.5 to 2.2 bar. To test the system, several inflation cycles have been performed and showed that the system presents good repeatability.

INDEX TERMS Battery-less, force-sensing resistor (FSR), near field communication (NFC), radio frequency identification (RFID), tire pressure sensor.

I. INTRODUCTION

NFC (Near Field Communication) has become an everyday technology for end-users, in contrast with other RFID (Radiofrequency Identification) protocols that are mainly used in industrial environments and require specific and expensive readers for communication. The growing popularity of NFCs is mainly due to their use in payment systems as well as the growing number of NFC-enabled devices and it is expected to continue being this way, especially given the desire to avoid using physical money as a result of the covid-19 pandemic [1]. The standardization of NFC started in 2004 when the NFC Forum [2] was created by the main mobile phone manufacturers, but it was not until a few years later, in 2010, that the technology started to be embedded in commercial mobile phones [3]. Nowadays NFC is used alongside other wireless technologies for the Internet of Things (IoT) such as Bluetooth, Wi-Fi and ZigBee. It employs an operational frequency of 13.56 MHz (f_{op}) and encompasses a wide range of applications such as healthcare [4]–[9], smart environment [10]–[14], social networks [15], [16], and payment [17], [18].

Batteries are present in many electronic devices, but they must be managed as hazardous waste because of their toxic contents or reactive properties [19], [20]. Rechargeable batteries (e.g. lithium-ion batteries) require additional specialized electronics for charging in order to extend the battery life, which increases the cost of the products. This in turn has

The associate editor coordinating the review of this manuscript and approving it for publication was Mohamed Kheir.

led to research into green energy sources and different energy harvesting strategies and technologies [21]–[23].

The most important NFC IC manufacturers have recently launched advanced integrated circuits (IC) with energy-harvesting capabilities [24]. These ICs convert part of the energy from the magnetic field generated by the NFC reader in order to provide a voltage output. This rectified output can power external electronic devices such as low-power microcontrollers or sensors. The progressive introduction of these ICs into the market enables the development of low-cost battery-less sensors. These devices can be used in sensing applications that must work over short ranges and for long periods because they must be available to be read on user request. Unlike other energy harvesting technologies, battery-less NFC-based sensors have the advantage that a current of up to a few mA (1-5 mA) can be obtained (with some external circuitry added to the NFC IC), which makes them readable using a standard smartphone [25]. Several examples of integration of NFC physical and chemical sensors with energy harvesting can be found in the literature [10], [11], [24], [26]–[30].

Since 2014, all cars in Europe have been equipped with a tire pressure monitoring system (TPMS) to identify under-inflation of the tires. This system directly measures tire pressure using battery-driven pressure sensors installed, most often, inside the valve of each wheel. Each sensor transfers the information by radio to a central control unit that reports it to the vehicle's on-board computer. The wireless communication is normally performed at 315 MHz or 433 MHz ISM bands and it is powered by a battery with a lifespan of approximately 5 years. When sensors are mounted inside the rim, they are no longer easily accessible to change the battery. Tires not only lose air if they get punctured, but they also lose air naturally. The main advantages of a TPMS are fuel savings, extended tire life, improved safety, and environmental efficiency. For this large market, several electronic manufacturers have developed specific highly-integrated tire pressure sensors such as the MLX91804 from Melexis [31], or the FXTH87 and NTM88 from NXP [32]. For older vehicles, external TPMSs are available that can be installed on the valve. The problem is that being an external element, it can be damaged or manipulated and the information can be lost. Sometimes indirect TPMSs are used. These indirect methods use velocity sensors installed in the antilock braking system (ABS) which indirectly measure the degree of inflation in the wheel. A tire spinning faster than normal is because its pressure is lower than recommended. With less pressure, the circumference of the tire is reduced.

Covid-19 not only changes the payment methods used, it also changes the lifestyle. The fact that healthcare authorities advised to avoid the use of public transports as well as a noteworthy increase of sports practice has made the bicycle market to increase significantly [33], [34]. A correct tire pressure is a determining factor to carry out a satisfactory activity. In the case of bicycle tires, the pressure depends on several factors such as the type of terrain, the size of the wheel, and the weight of the cyclist. Improper tire pressure can result in tire puncture, uneven tire wear or inefficient traction.

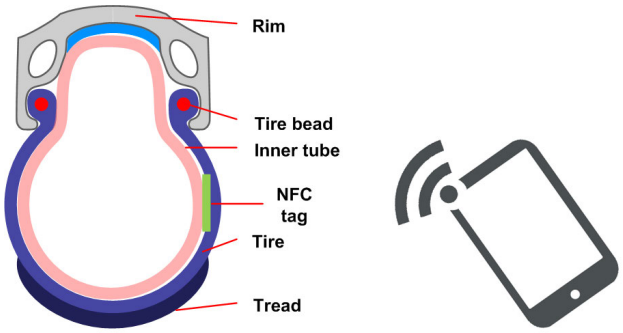

FIGURE 1. Tire diagram with the tag installed between the inner tube and the tire.

Due to the high growth in the market associated with bicycles and their accessories, aftermarket TPMS units (e.g. SYKIK Rider SRTP670 [35], FOBO 2 Bike TPMS [36], Garmin Zümo TPMS [37]) for bikes and motorcycles have become commercially available. External sensors are placed on the valve stem. These TPMS can read the pressure and temperature of the tires and then transmit the information via Bluetooth low energy (BLE) or through ANT technology to a specific device or to a smartphone within the Bluetooth range. The sensor detects slow or fast leaks and sends alerts to the user. The sensors are relatively easy to install and maintain, but they are expensive (about 100 $). In addition, they can be stolen if they do not have a locking mechanism, they protrude slightly, they must be removed to inflate the tire, their accuracy can be affected by weather conditions and their batteries need to be replaced. Consequently, these sensors are waterproof and are often secured with lock nuts to prevent theft. But these locking systems lead to difficulties when inflating the tires. This make an internal low-cost battery-less TPMS for bicycles a promising idea.

In [38] an NFC bicycle tire pressure measurement system (BTPMS) was proposed. It was based on an application-specific integrated circuit (ASIC) with pressure measurement capability. The ASIC consists of a microelectromechanical system (MEMS) capacitive sensor and an ISO 14443 RFID interface. The capacitive sensor is based on a micromachined cavity that bends due to the air pressure. This means that the sensor must be installed within the inner tube, thus requiring a special tube design. Unlike [38], the present study presents a system that uses commercial off-the-shelf (COTS) components that can be installed by the user between the tire and the inner tube (see Fig. 1). It is therefore compatible with conventional bicycle tires and can be reused. This work studies the feasibility of measuring tire pressure using a battery-less NFC sensor based on a force-sensing resistor (FSR).

The present study is organized as follows. Section II describes the system and its components. Section III presents the proof-of-concept prototype along with details about the

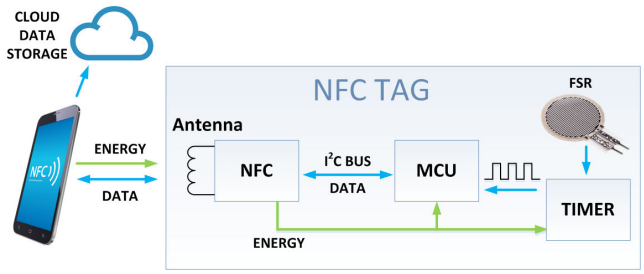

FIGURE 2. System overview block diagram.

antenna design and the procedure for tuning the tag. Experimental results regarding the read range and sensor characterization obtained with this prototype are shown in Section IV. Section V compares the proposed device with other TPMS technologies. Finally, section VI contains the conclusions.

II. SYSTEM OVERVIEW

A block diagram of the proposed system is depicted in Fig. 2. It consists of a passive NFC tag which retrieves the energy from the reader (i.e. any NFC-enabled device) by rectifying the radiofrequency field, thus obtaining a voltage capable of powering the tag circuitry. The RF to DC conversion is carried out internally by the NFC integrated circuit (IC) with energy harvesting capability. For this study, the NTAG NT3H2111 from NXP has been used. The NFC IC is connected to a microcontroller which obtains the value measured by the force-sensing resistor (FSR), calculates the tire pressure, and writes the result to the NFC IC EEPROM, which is then retrieved by the reader and shown to the user. The microcontroller and the NFC IC communicate using the I^2C protocol. The tire pressure is obtained by measuring the resistance of the force-sensing resistor (FSR), which controls a variable controlled oscillator implemented with a low-power 555 timer. Thus, a frequency that depends on the force applied to the FSR's sensing area is obtained. For the proposed application this method is more accurate and has a higher operating range than the method proposed by the FSR manufacturer, which is based on a voltage divider and an operational amplifier. Furthermore, since most modern smartphones are NFC enabled, they can be used as NFC reader. Both the measured pressure value and that recommended by the manufacturer can be shown in the mobile display. Also, the measured pressure can be uploaded to the cloud via Wi-Fi or the mobile network.

A. FORCE-SENSING RESISTOR

Force-sensing resistors (FSR) are devices whose resistance changes when a force is applied to them [39], [40]. FSRs have been used for different applications such as measuring the distribution of force in hands [41], [42] and feet [43], digital music instruments [44] and muscle activity [45]. FSRs present a power law behavior whereby resistance decreases as applied force increases. This translates into high accuracy

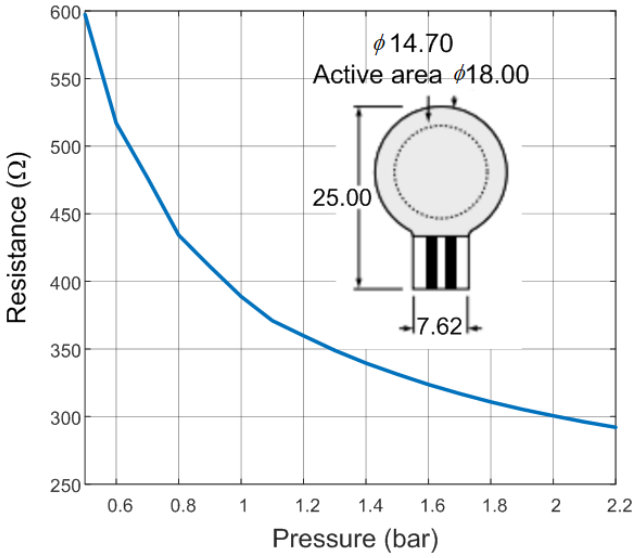

FIGURE 3. Resistance change due tire pressure. The inset shows the shape and size of the FSR06 from Ohmite (dimensions in mm).

for small force measurements but makes it difficult to achieve acceptable accuracy for large force measurements. The simplest conditioning circuit recommended by the manufacturer consists of using the FSR as part of a voltage divider, converting resistance changes into voltage changes. For applications where it is necessary to work with large forces, manufacturers suggest the use of operational amplifiers. However, it must be taken into account that there is a trade-off between the increase in the amplifier and the force range in which it is possible to measure.

Due to the internal tire pressure (P), the active surface of the FSR (S) supports a force $F = P{\cdot}S$. The Ohmite FSR series that can sense forces up to 5 kg has been chosen and the specific sensor used in the prototype is the FSR06 with an active area diameter of 14.7 mm, a thickness of 0.375 mm, and an overall size of 18 × 25 mm (see the inset picture in Fig. 3). Fig. 3 depicts the measured resistance of the sensor (R_{FSR}) as a function of the applied pressure. The maximum force specified by the manufacturer that can support the sensor is 5 kg, which corresponds to a maximum pressure of 2.9 bar (1 bar = 100 kPa) and is close to the maximum tire pressure used in the experiments (59 mm-width mountain bike tire). The tire pressure range depends on its physical characteristics and its thickness. For high tire pressures, an FSR with a small active area can be used. For instance, the FS04 model from Ohmite supports the same force but presents an active diameter of 5.6 mm, achieving a maximum pressure of 20 bar.

The FSR is inserted in a bike wheel between the inner tube and the tire. The pressure is measured with a manometer while the tire is inflated with an electronic pump. Simultaneously, the resistance is measured with a multimeter connected to the FSR. It can be seen that the resistance decreases with the pressure applied. For pressures under 0.3 bar, the FSR acts as an open circuit, at 0.5 bar $R_{FSR} = 597\ \Omega$, and

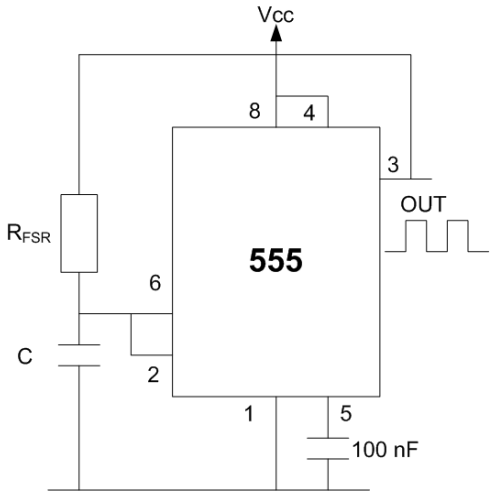

FIGURE 4. Scheme of 555 timer-based oscillator used to measure the resistance of the FSR.

at 2.2 bar $R_{FSR} = 292\ \Omega$. The FSR is connected to a 555 timer in order to obtain a frequency as a function of the pressure applied. This configuration is selected instead of another based on a Wheatstone bridge (consisting of three known resistors, the FSR and an operational amplifier) to achieve better accuracy for high pressure values. The approach based on the Wheatstone bridge presents two main problems. The first is related to the operational range, since the increase of the gain necessary to improve the resolution in the high-pressure range, leads to a reduction of the operating range of the system, which implies an increase in the complexity of the circuitry needed to measure different intervals. The second problem is the hysteresis, which has been addressed in the literature [46]–[49]. These studies show that resistance to the frequency circuit reduces the effect of hysteresis. The manufacturer specifies a part repeatability of 2% and a hysteresis of 5%. The 555 has been configured in a simple mode (see Fig. 4), with $C = 1\ \mu F$. In the present study, a simple classical low-power CMOS ICM7555 was chosen for the prototype. The current consumption is typically 80 μA at 3 V. However, advanced timers with low current consumption such as an oscillator based on low-power NAND gates can be used as an alternative [50] and are commercially available. Another alternative is to use a low-power opamp oscillator. However, CMOS 555 is characterized by an exact 50% duty cycle and an oscillation frequency independent of the power supply voltage (unlike the opamp circuit-based oscillator). Finally, another alternative is modern micropower oscillators such as the LTC6907 from Linear Technology, which consumes 33 μA when powered at 3 V. As the capacitor charges and discharges through the same resistor, the duty cycle of this basic arrangement is very close to 50%. The square wave output pulses have a period equal to approximately $2ln(2)R_{FSR}C$. The output frequency (f_{out}) is therefore given by (1):

$$f_{out} = 0.722/(R_{FSR} \cdot C) \tag{1}$$

The output frequency therefore depends on the resistance of the FSR, which in turn depends on the tire pressure (see Fig. 3). Thus, the expected frequencies range from 1209 Hz at 0.5 bar ($R_{FSR} = 597\ \Omega$) to 2472 Hz at 2.2 bar ($R_{FSR} = 292\ \Omega$). Taking into account that the target resolution should be in the order of 0.1 bar, the smallest step occurs for higher pressure values. The difference between 2.1 bar ($R_{FSR} = 295\ \Omega$, $f_{out} = 2443\ Hz$) and 2.2 bar ($R_{FSR} = 292\ \Omega$, $f_{out} = 2472\ Hz$) is about 29 Hz whereas at the lowest pressure (between 0.5 and 0.6 bar) the step is 277 Hz.

B. MICROCONTROLLER

In order to measure the change in frequency caused by the change of R_{FSR}, a microcontroller (MCU) is required. As explained above, the proposed system harvests the energy from the RF signal generated by the reader; therefore, the available power is limited and the MCU must be a low-power component to stay within the system constraints. The selected MCU is the ATtiny85 from Atmel, which is a low-power AVR 8-bit microcontroller. It can work with 1.8 V, and consumes 300 μA at 1.8 V and 500 μA at 3 V when it is configured to the lowest clock frequency (i.e. 1 MHz). Although there are other 8-bit microcontrollers in the market with similar features, this has been chosen for its availability, ease of programming with the Arduino IDE and low cost. The ATtiny85 performs three differentiated functions which are explained below.

1) FREQUENCY MEASUREMENT

Since pressure detection is based on a change in frequency, a frequency measurement method is required to calculate the tire pressure. Different methods to implement a frequency counter with an MCU can be found in the literature [51]. The one chosen for this project is based on the external interrupt capability of the ATtiny85. The frequency-dependent signal obtained from the 555 timer output is connected to the interrupt pin of the MCU. The frequency is obtained from the inverse of the period. The period is obtained with the function pulseIn, available in Arduino libraries, which measures the time that the signal in a pin remains at high or low level. Therefore, the period is the time interval that the signal is in high level plus the time interval that it remains in low level during each cycle. This method consists of measuring the time between rising cycles. The measurement is taken 5 times and then averaged to obtain the input frequency. Accuracy under 1 Hz is obtained for the input frequency range required (1200 Hz to 2500 Hz approximately).

2) COMPUTATION

The measured frequency can be stored and formatted to be retrieved by the reader, which may result in a frequency to pressure conversion on the reader side. Although the computational capability of the readers is much higher than that of the ATtiny, this would require a specific application in the reader in order to obtain the final value. The proposed system is intended to be independent of the reader model.

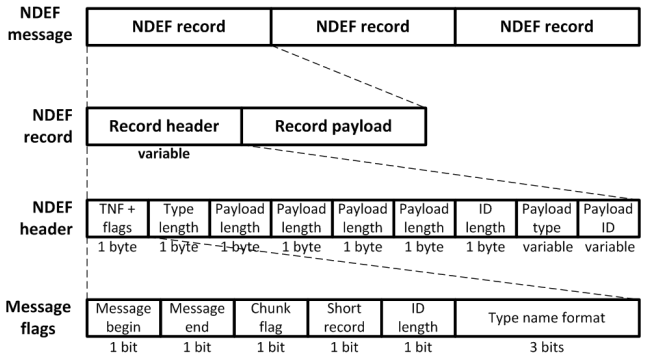

FIGURE 5. NDEF message structure.

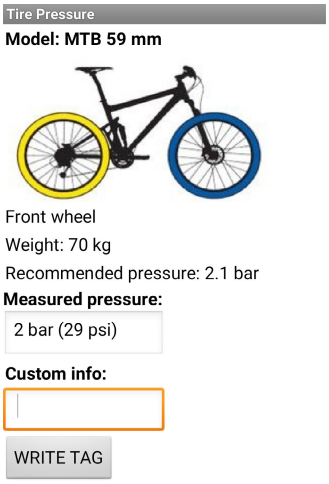

FIGURE 6. Scheenshot of a simple Android application.

Consequently, it must not be necessary to install any specific application on the reader. Therefore, the ATtiny converts the measured frequency to pressure, calculated in bar, by a second-order polynomial. The benefit of this approach is that the NFC's IC memory stores the final value, which means that the user obtains the result immediately by simply reading the tag with any NFC-enabled device. This makes the system reader-independent. In contrast, if the raw data was stored (i.e. the frequency), that would force the system to use a specific application on the reader side. Storing the raw data would allow external calibrations of the sensors (not required in the present study) rather than having the tag calibrated for a specific application.

The pressure obtained is then formatted to NDEF (NFC Data Exchange Format) [52]. NDEF is a standardized data format (by the NFC Forum [2], [53]) used to exchange data between any compatible NFC device and another NFC device or tag. An NDEF message consists of one or more NDEF records, and each record is formed by a header and a payload (see Fig. 5) [53]. In order to format the data, the MCU calculates the required header and message flags (type length, payload length, ID length) and sends the resulting message through the I^2C bus to be stored in the NFC tag IC EEPROM memory. In addition to the pressure, additional information related to the tire can be stored in the NDEF message.Although the NDEF message recorded in the EEPROM can be read with any NFC reader, a mobile app has been designed to add new functionalities based on the information stored at the tag. Fig. 6 shows an image of a simple Android application that shows the measured pressure obtained from the NDEF message and writes some additional information in the tag. Depending on the tire model obtained from an identification code that can be stored in the NDEF message, either in the front or rear wheel, and on the pressure level recorded, the app can help decide the optimal pressure level based on the cyclist's weight.

C. NFC TAG IC

The NFC tag IC is responsible for carrying out the communication with the reader as well as providing a rectified voltage to the tag circuitry. The capability of providing a rectified voltage from the RF signal is known as energy harvesting (EH). The main NFC IC manufacturers offer ICs with EH capability. The one selected is the NT3H2111 (NT3H) from NXP Semiconductors. It is a Type 2 Tag ISO/IEC 14443A compliant, with a transmission rate of 106 kbps, I^2C interface, 2 kbytes EEPROM (write endurance minimum 500.000 cycles), internal capacitance of 50 pF, and a unique 7 byte UID. The current consumption of the NT3H is 240 μA.

The NDEF message sent by the MCU and received through the I^2C bus is stored in NT3H's EEPROM memory. Once an NFC reader initiates the communication with the tag, the NT3H uses the information stored in the EEPROM to modulate the signal received by using the back-scattering modulation technique [24].

III. PROTOTYPE

The prototype designed has been manufactured on an FR4 substrate (with a substrate thickness of 0.8 mm) and is shown in Fig. 7. The use of a semi-rigid substrate allows the SMD components to be assembled, thus preventing the impact of these components due to the pressure and improving the repeatability of the measurement with the FSR. However, to prevent the tire from being punctured, a 3D printed enclosure has been designed and manufactured using a flexible thermoplastic elastomer TPEE. The purpose of this prototype is to show the feasibility of the power transfer and the battery-free pressure sensing capability of a tag using a miniaturized antenna. The overall tag dimension is 14 $\times$ 48 mm. All the SMD components are welded on one side of the PCB, leaving a flat face where the FSR is placed. The overall current consumption is under 1 mA and the cost is around 6$ due to the cost of the FSR. A capacitor of 200 nF is connected between the rectified voltage output and the ground to ensure that the voltage does not drop during modulation or during any application operation. 15 kΩ pull-up resistors are placed in both I^2C lines between the microcontroller and the NFC IC.

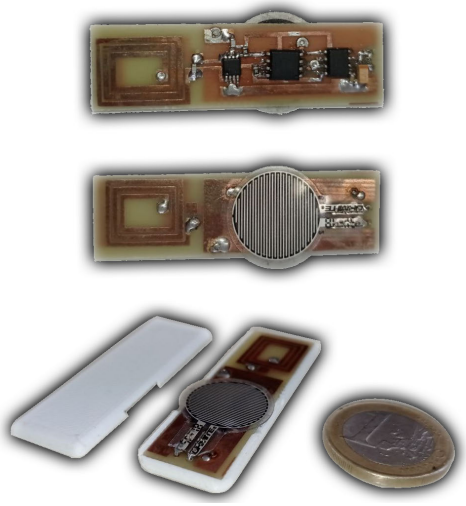

FIGURE 7. Photographs of both sides of the tag prototype consisting of a 12 × 16 antenna, an NFC chip, a microcontroller, a 555 timer, and an FSR. Overall dimensions of 14 × 48 mm.

TABLE 1. Antenna parameters.

Symbol	Description	Value
L_1	Antenna width (mm)	12
L_2	Antenna height (mm)	16
A	Area (mm^2)	192
N	Turns	6
PS	Printed sides	2
w	Trace width (mm)	0.8
s	Spacing between traces (mm)	0.5
h	Substrate thickness (mm)	0.8
ϵ_r	Relative permittivity	4.7
mh	metallization thickness (μm)	34
f_r	Self-resonance frequency (MHz)	172.8
L	Inductante at 13.56 MHz (nH)	411
Q	Quality factor at 13.56 MHz	81

A. ANTENNA DESIGN

The tag coil antenna is a crucial element for communication. Its electrical and geometrical parameters are detailed in Table 1 and determine the maximum operational read range. It is important to note that the magnetic coupling efficiency is very sensitive to the alignment of the primary and secondary coils and to the distance between them, because the magnetic field decays as $1/r^2$, being r the distance between coils. The best coupling is found when both antennas, reader and tag, have the same size. However, the proposed application requires a smaller device than the average antenna size used, for example, in payment cards. A good antenna design is essential because of the huge variety of reader antennas available. When designing the NFC tag, in contrast to other RFID systems which use well known antennas, it has to be kept in mind that most readers are likely to be commercial cellphones, and that each manufacturer uses different techniques to design their antennas. Therefore, any miniaturized antenna must be carefully analyzed to ensure the best possible performance in the smallest feasible size. The proposed antenna has been modeled and simulated using

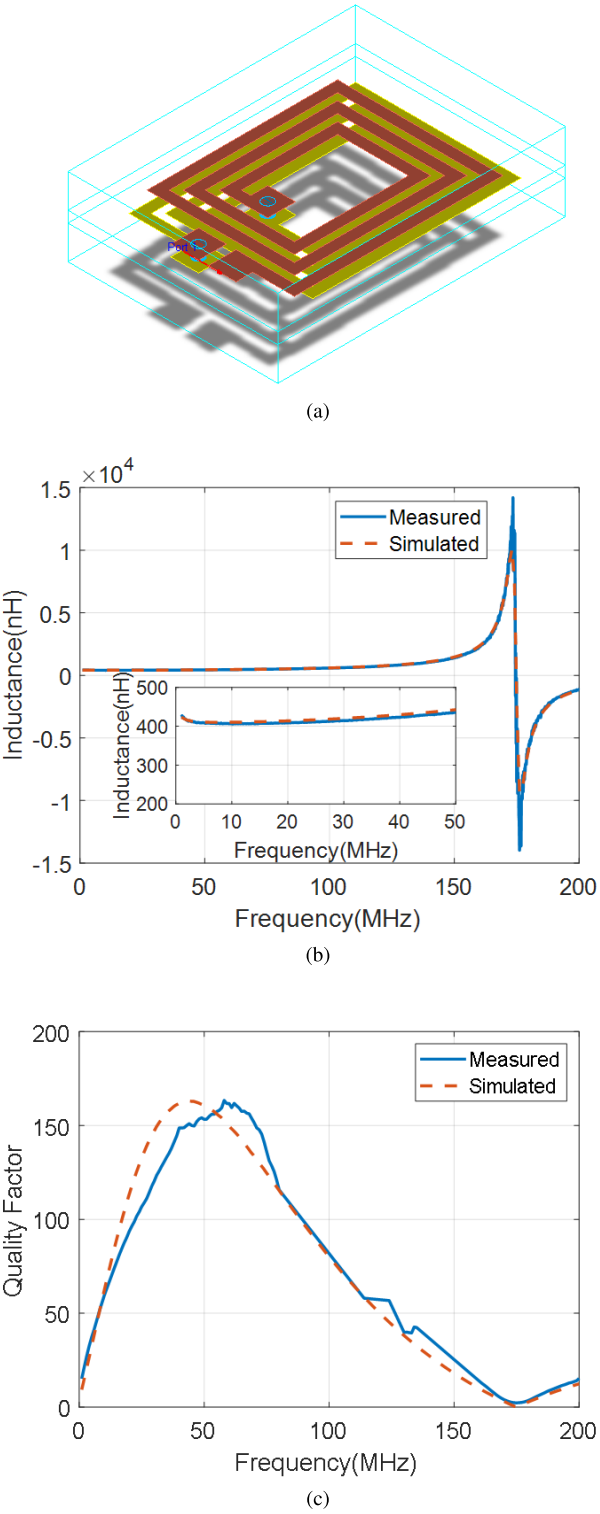

FIGURE 8. (a) Antenna 3D model, (b) measured and simulated inductance and (c) quality factor.

ADS by Keysight and the electromagnetic simulator tool Momentum.

Fig. 8(a) shows the designed layout. Given the location of the tag within the wheel, a rectangular shape has been used. A prototype of antenna connected to an SMA coaxial

connector has been measured (blue square in Fig.10(a)). After de-embedding the delay inserted by the connector, the antenna equivalent inductance L is computed from the impedance parameters using expression (2):

$$L = \frac{Im(Z_{11})}{2\pi f} \tag{2}$$

where $Im(Z_{11})$ is the imaginary part of Z_{11} and f is the frequency. Expression (3) is used to compute the antenna quality factor (Q), which determines the bandwidth:

$$Q = \frac{Im(Z_{11})}{Re(Z_{11})} \approx \frac{2\pi fL}{R} \tag{3}$$

where $Re(Z_{11})$ is the real part of Z_{11}. Fig. 8(b) and Fig. 8(c) compare the measured and simulated inductance and the quality factor, respectively. The coil quality factor increases more or less linearly at low frequency. In this range the quality factor is determined from the inductance reactance and the equivalent antenna resistance. This resistance depends on the frequency due to the skin effect and increases with frequency [25]. The presence of the parasitic capacitance between the strips decreases the coil reactance as the frequency increases. This effect produces a peak in the quality factor. The frequency of this peak is difficult to adjust because of its dependence on the parasitic capacitance (which is difficult to control). In general, small printed inductances make it possible to reduce the resistance of the antenna, thus increasing the quality factor. For our coil design, the measured inductance and the quality factor are 408 nH and 72.3 at 13.56 MHz, respectively, which agrees well with the simulated values, 411 nH and 81. The resonance frequency of the unloaded antenna is f_r=175 MHz. Using the resonance frequency and the low-frequency inductance, the equivalent parallel parasitic capacitance C_p can be calculated thus:

$$C_p = \frac{1}{(2\pi f_r)^2 L} \tag{4}$$

A value of C_p=2 pF is found. This value is used to adjust the tuning capacitance. Note that, unlike conventional wireless power transfer systems dedicated to wireless charging, in NFC the Q is limited to ensure that sidebands containing the information are not degraded. Therefore, the requirements for coils with high quality factors can be relaxed and even low quality factor inkjet-printed coils have been proposed for low-cost tags in NFC applications [54]. The equivalent circuit for the tag antenna is shown in Fig. 9 [24]. The series resistance, which takes into account the skin effect, is modeled with the series resistance R [25]. The equivalent parallel resistance R_p can be calculated from the series antenna resistance ($R = 0.4\Omega$), the extracted inductance ($L = 411\ nH$) at low frequency and the resonance frequency ($f_r = 175\ MHz$) [24]:

$$R_p = \frac{(2\pi f_r L)^2}{R} \tag{5}$$

A value of $R_p = 510.6\Omega$ has been obtained.

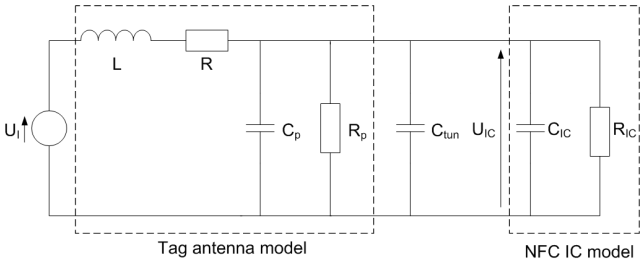

FIGURE 9. Tag equivalent circuit for wireless power transfer considerations.

B. TAG TUNING

The time-variant magnetic flux generated by the reader produces an induced voltage (U_I) in the tag coil antenna. The voltage (U_{IC}) at the input of the NFC IC depends on the loop inductance, the parasitics, and the equivalent IC input elements as shown in Fig. 9 [24], [55]. The NFC IC input impedance is modelled as a parallel-connected capacitance and resistance. The voltage at the input is maximized at the resonance frequency of the tag which, once rectified, can be used as power coming from an energy harvesting system. Therefore, the tag's resonance frequency must be tuned to the NFC operation frequency (13.56 MHz). This resonance frequency can be obtained by analyzing the tag equivalent circuit of Fig.9 [55]. and depends on the inductance and capacitance of the antenna, as expressed in (6):

$$f_r \approx \frac{1}{2\pi\sqrt{L(C_{IC} + C_p + C_{tun})}} \tag{6}$$

where C_{IC} is the NFC tag IC capacitance (typically 50 pF for the NT3H2111), C_p is the parasitic capacitance, and C_{tun} is a tuning capacitance connected in parallel to the antenna in order to adjust the resonance frequency of the tag (f_r) to the operational frequency of NFC ($f_{op} = 13.56\ MHz$). The effect of the small series resistance R and the large parallel resistance R_p is small at the resonance frequency of the tag. Therefore, as a first approximation, these components can be neglected (see 6) [24], [55]. The tire and the protection box are made with nonmagnetic materials, therefore the proximity of the antenna to the tire does not modify its inductance with respect to the case of free-space, but increases the parasitic capacitance due to the presence of the dielectrics. Furthermore, the metallic strip to interconnect the antenna and the NFC IC introduces a small deviation in the parasitic capacitance and the inductance of the antenna. As the tag is semi-rigid the effect of pressure and bending is negligible. Therefore, a fine adjustment has been experimentally carried out by using a vector network analyzer and measuring the resonance frequency with a probe coil close to the tag following the procedures described in [24]. The resulting value of C_{tun} is 270 pF.

IV. EXPERIMENTAL RESULTS

A. ENERGY HARVESTING RANGE

For the nominal current load, a minimum field strength is required for a stable operation that determines the energy

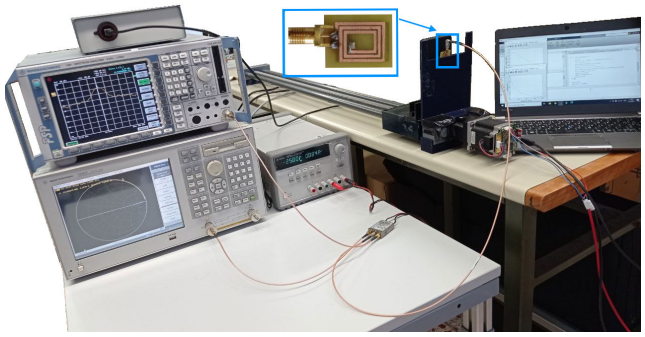

(a)

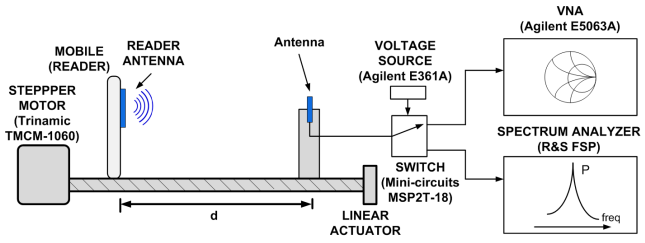

(b)

FIGURE 10. (a) Image of the setup to measure the magnetic field received by the tag antenna. (b) Schematic of the setup.

harvesting range. For long distances, the NFC IC is unable to provide a minimum voltage to wake up the microcontroller and therefore only previously measured sensor values saved in the NFC EEPROM can be read. In order to determine the energy harvesting range, an experimental setup has been developed [25]. Fig. 10 depicts the setup used to measure the behavior of the antenna while it is illuminated by a reader at different distances. To be more like a real situation, a smartphone with a metallic case is used as a reader in order to take into account tag detuning. Fig. 10(a) shows a picture of the setup, comprising a Xiaomi Mi Note 2 as a reader, the 16 × 12 mm antenna connected to a spectrum analyzer and to a VNA (Vector Network Analyzer), and a linear actuator governed by a stepper motor to control the distance between the reader and the antenna. A personal computer was used to control the motor and the instruments through GPIB (General-Purpose Instrumentation Bus) to automatize the procedure of measuring the parameters for each distance.

Fig. 11 displays the power received by the antenna at 13.56 MHz, which decreases linearly with distance (d). Using the measured power, the voltage generated on the coil terminals (V_{RMS}) can be obtained and used in (7) to calculate the average magnetic field received by the tag (H_{AV}):

$$H_{AV}(A_{RMS}/m) = V_{RMS} \cdot |AF| \tag{7}$$

with $|AF|$ being the antenna factor expressed as (8) [56]:

$$AF = \frac{Z_0 + Z_{in}}{j2\pi f_{op}\mu_0 Z_0 AN} \tag{8}$$

where Z_0 and Z_{in} are the reference and input impedances, fop the operational frequency (13.56 MHz), μ_0 the permeability of the vacuum, A the loop area, and N the number of turns

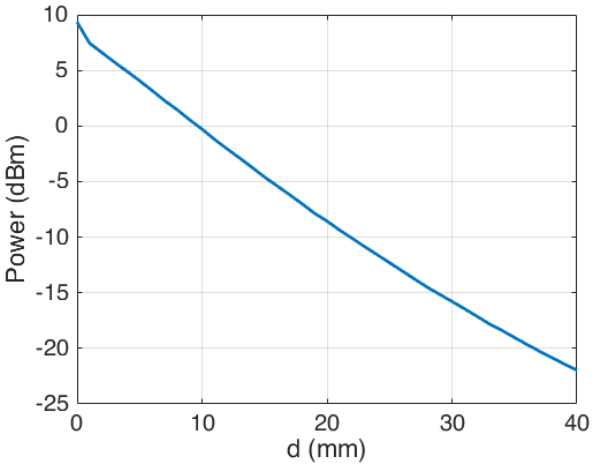

FIGURE 11. Measured Power as a function of the distance from the tire.

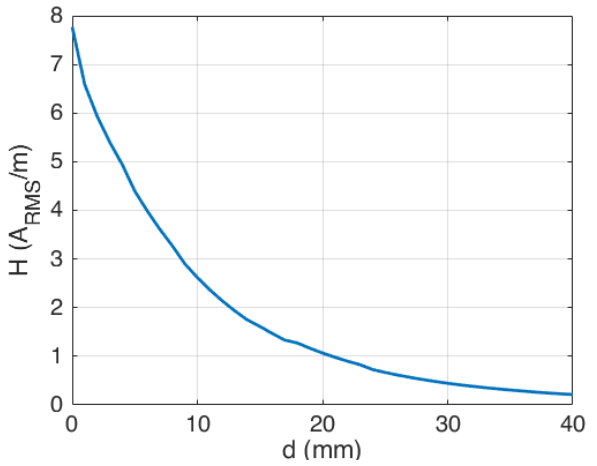

FIGURE 12. Measured Average Magnetic field as a function of the distance from the tire.

of the antenna. Fig. 12 shows the measured average magnetic field as a function of the distance from the tire.

The presence of the reader near the tag leads to undesirable effects due to its metal parts, decreasing the tag antenna's inductance (L), as can be seen in Fig. 13. Additionally, the antenna is detuned, increasing the tag resonance frequency [24]. Without the presence of metal, the inductance measured at 13.56 MHz is $L = 408\,nH$, and the quality factor is $Q = 72.3$. The ISO/IEC 14443A specification determines the maximal value of Q_T as $f_{op}/(2 \times bitrate)$, which leads to a maximum allowed Q_T of 64. However, that refers to the total quality factor of the tag (Q_T), taking into account the quality factor associated with the NFC tag IC (Q_L). Thus, the total quality factor of the tag Q_T can be expressed as (9):

$$Q_T = \frac{QQ_L}{Q + Q_L} \tag{9}$$

$$Q_L = \frac{R_{IC}}{2\pi f \cdot L} \tag{10}$$

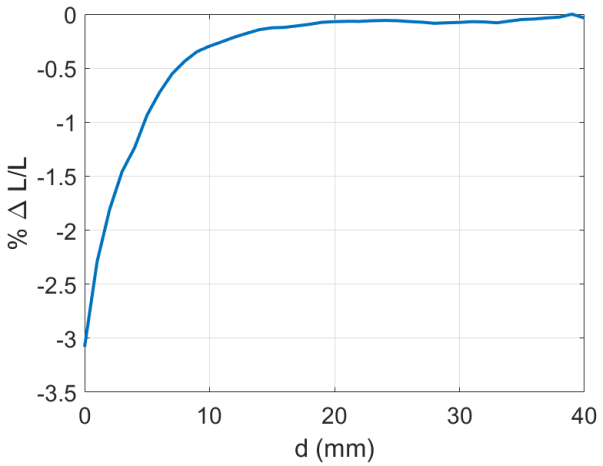

FIGURE 13. Measured variation of inductance as a function of the distance to the reader (mobile phone) at 13.56 MHz.

where R_{IC} is the equivalent resistance of the NFC IC. This resistance is nonlinear and depends on the input voltage to the IC. Typical values are in the order of 500-1000 Ω for NFC IC with energy harvesting [25]. Therefore, the total Q_T factor is determined by the IC Q_L factor because it is smaller than the typical quality factor of the coil antenna. Whereas a high Q_T value benefits the power transfer, it reduces the bandwidth (BW), as can be deduced from (11):

$$BW = \frac{f_{op}}{Q_T} \tag{11}$$

Due to the low value of Q_L, the tag does not filter the modulated sidebands and the maximum total quality factor requirement can be fulfilled.

In addition to modifying the inductance and quality factor, the proximity of the reader to the tag detunes the antenna, so that as the reader gets closer a higher resonance frequency (f_r) is obtained. This fact must be considered when tuning the antenna. The resonant frequency of the tag should be set slightly below the operating frequency to account for the inductance reduction due to the presence of the reader.

The energy harvesting range determines the maximum distance between reader and tag to receive enough RF signal to generate a DC current. This range is fixed by the minimum average magnetic field required to activate the chip (H_{min}) (12) [55]:

$$H_{min} = U_{min} \frac{\sqrt{\left[1 - (\frac{f_{op}}{f_r})^2\right]^2 + \frac{1}{Q_T^2}}}{2\pi f_{op} \mu_0 A N} \tag{12}$$

where U_{min} is the minimum voltage required for the tag operation, which depends on the chip IC. From (12) it should be noted that this value depends on the size of the antenna used and the IC model. H_{min} depends on the IC resistance, therefore, it is nonlinear and depends on the distance. Furthermore, U_{min} depends on the DC load at the energy harvesting output. Therefore, H_{min} depends on the load connected to the NFC IC. H_{min} was experimentally measured using a voltmeter

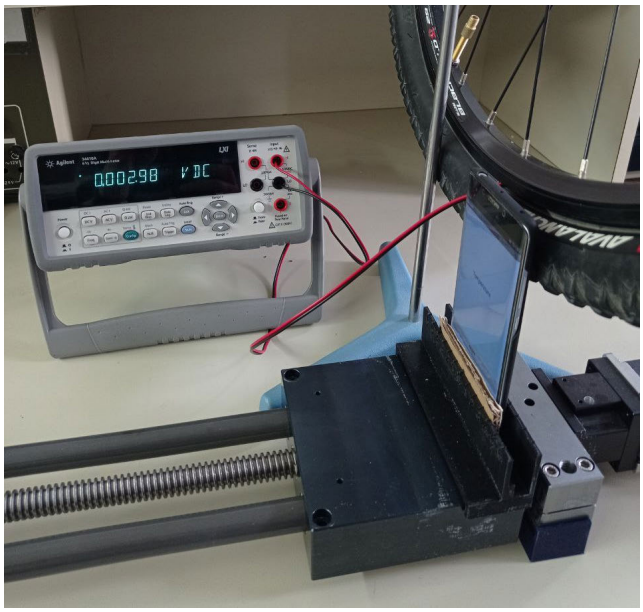

(a)

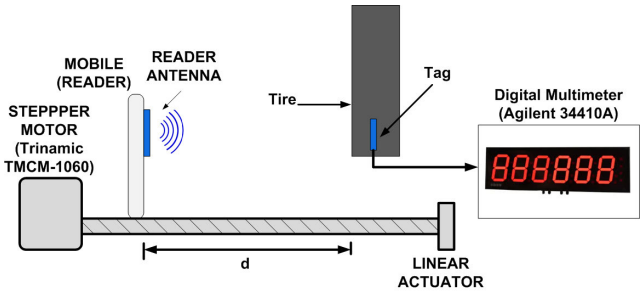

(b)

FIGURE 14. (a) Image of the setup to measure the energy harvesting output of the tag. (b) Schematic of the setup.

connected to the rectified voltage output (V_{DD}) of the NFC tag (Fig. 14(b)). The tag was placed between the tire and the inner tube, and the reader was centered parallel to the tag. As can be seen in Fig. 14(a), the rectified output voltage obtained is 2.98 V. This value remains constant for distances up to 8 mm between the reader and the outer part of the tire. For values higher than 8 mm, the magnetic field received is lower than H_{min} and, therefore, V_{DD} is not activated. Knowing that the maximum distance is 8 mm, and adding one more mm due the tire, H_{min} may be obtained from Fig. 12, meaning that when this chip (NT3H) is connected to this antenna, the minimum magnetic field required for it to operate is about 2.9 A_{RMS}/m.

B. SENSING

This section reports the tests performed with the tag inserted inside the tire. The first one consists of taking 100 samples for each 0.1 bar step while the tire is inflating. Fig. 15(a) depicts the result, with a different color for each step. Another test shown in Fig. 15(b), demonstrates the repeatability by repeating three inflation cycles up to 1 bar, waiting for a while, inflating up to 2 bar, waiting for another while, and then completely deflating the tire.

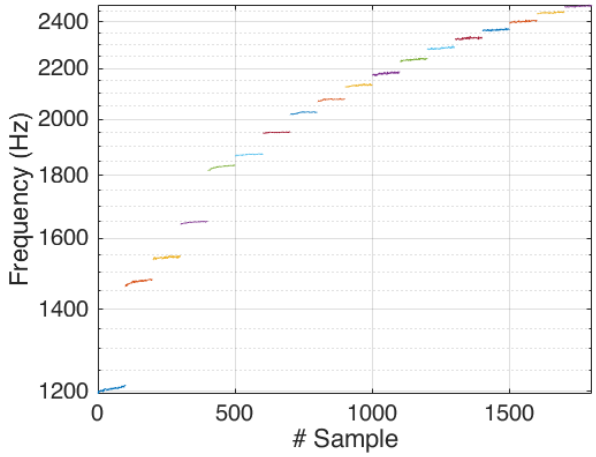

(a)

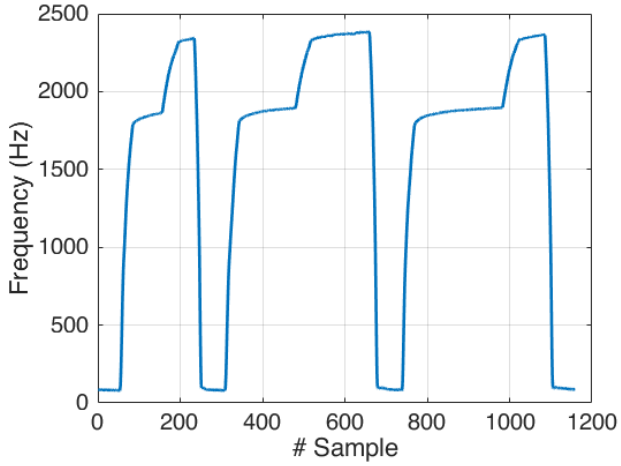

(b)

FIGURE 15. (a) 100 measurements for pressures from 0.5 to 2.2 bar every 0.1 bar. (b) Three inflation cycles from 0 to 2 bar, stopping for a while at 1 bar, and deflating 3 times.

Fig. 16 shows the relationship between the measured tire pressure and the oscillation frequency. A polynomial fitting has been calculated and implemented in the microcontroller, and is expressed as (13):

$$P(bar) = 1.95 - 2.36 \cdot 10^{-3} \cdot f_{out} + 9.9 \cdot 10^{-7} \cdot f_{out}^2 \quad (13)$$

where f_{out} is the measured output frequency of the 555 timer oscillator in Hz. A correlation coefficient $R^2 = 0.998$ was obtained considering this polynomial fitting. Fig. 16 also compares the measured pressure and the second order polynomial fitting curve as a function of the oscillator frequency.

V. DISCUSSION

This section compares the proposed system with other direct TPMS technologies. Table 2 shows some selected TPMS technologies and their main characteristics. In recent years, the development of MEMS (MicroElectroMechanical Systems) pressure sensors [57] has allowed for the development of commercial TPMS systems for cars. These sensors are based on capacitive sensing using micromachined suspended

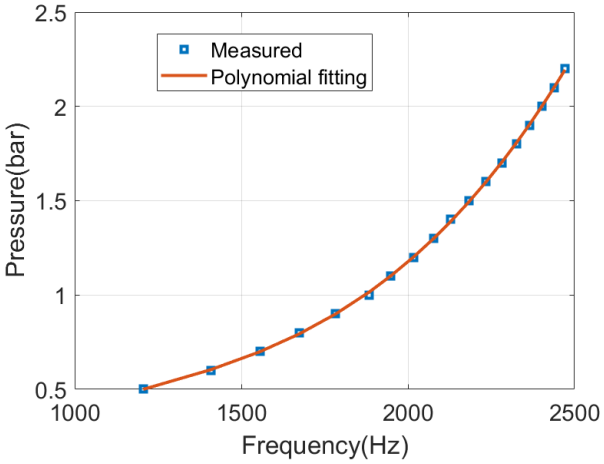

FIGURE 16. Measured relation between pressure and frequency (blue line), and the second order polynomial fitting curve (red line).

membranes, which are deflected towards the bottom electrode with the increase in pressure, resulting in a reduction in the distance between electrodes and increasing the capacitance. This technology is compatible with CMOS processes, resulting in several commercial ICs on the market that combine the sensor, ADC, microcontroller and RF interface. These TPMS sensors are mainly designed for cars and they are installed inside the valve. A transmitter at 315 MHz is used in the USA whereas a transmitter at 433 MHz is used in the EU. An LF link at 125 kHz is often used for external configuration. Examples of modern ICs are then MLX91804 from Melexis [31], or the FXTH87 and NTM88 from NXP [32]. These sensors are designed for tubeless tires and cannot be installed in conventional bicycles tires due to their size. Currently, the market is mainly supplied with direct-battery TPMS, which is shipped with batteries. The main limitation of these sensors is the lifespan of the battery, which must be changed regularly, thus increasing the maintenance cost. Some studies have proposed harvesting energy from triboelectric nanogenerators [58] or from mechanical vibrations [59]–[62]. Battery-less implementation schemes have become a trend in TPMS, with energy harvesting from wireless power transfer in the 13.56 MHz link has been studied together with high-efficiency transmitters [63], [64]. It should be noted that these systems are designed to operate in cars where a specific reader can be placed to send the information to the onboard control system. They are difficult to apply to bicycles or even motorcycles.

The problem of replacing batteries is mitigated for external TPMS devices installed in the valve. Versions for cars, motorcycles and bicycles are found in the market. However, these devices must be equipped with anti-theft lock systems, which makes it difficult to inflate the tire. Different wireless systems can be found with ASK/FSK modulation at 315/433 MHz ISM bands and low-power radios such ANT or recently BLE, which enable the data to be received on the smartphone. Besides TPMS with batteries, some battery-less sensors have also been proposed in the literature. In [65] a chipless RFID

TABLE 2. Comparison with other TPMS techcnologies.

Ref.	Technology and Commun.	Vehicle	Comment
[31], [32]	Integrated MEMS and 315/433 MHx Tx	car, internal	Battery based IC devices MLX91804 from Melexis and FXTH87/NTM88 from NXP
[66]	Freescale MPX5500 and Bluetooth	car, stem valve	distance 10-15 m
[35], [36]	Bluetooth LE	motocycle and bike	Battery, commercial devices SYKIK Rider SRTP670 and FOBO2
[37]	ANT 2.45 GHz	motocycle and bike	Battery, commercial devices Garmin Zumo
[63], [64]	WPT at 13.56 MHz and Tx at 433 MHz	car, inside	Batteryless with wireless Power Transfer at 13.56 MHz
[65]	passive SAW resonator at 433 MHz	car, stem valve	Batteryless. Measurement pressure from frequency resonance shift
[38]	MEMS sensor and NFC	tubeless tire, bike	ASIC ISO 14443 standard, FR4 substrate, 35x15 mm coil
this work	FSR sensor and NFC	bike, internal	ISO 14443 COST components, FR4 substrate, 16x12 mm coil

system is proposed, in which a passive SAW-based resonator is remotely interrogated to read out the tire pressure information at 433 MHz.

Battery-less NFC-based tire sensors have also been proposed in the literature. In [38] an integrated NFC ASIC compatible with ISO14443A and featuring a MEMS pressure capacitive sensor is proposed. The tag consists of a 35 × 15 mm coil made of FR4 substrate connected by wire bonding to the ASIC. The device is designed to be placed inside of the tire in tubeless tires. In the present study, an NFC sensor using commercial COST components (standard NFC NXP NTAG and low-cost microcontroller) has been proposed. Its advantage is that can be used with conventional tires (not tubeless). The use of COST components reduces the time to market compared to the use of specific ASICs, which require large quantities to be cost-effective. However, battery-less NFC devices only can measure in presence of the reader (e.g., an NFC-enabled smartphone). Therefore, continuous pressure monitoring is not possible. In the case of bicycles, the main application is to check the pressure state to decide if it needs to be adjusted especially if a low-cost portable bicycle stain (sometimes without a manometer) is used. As these devices are installed inside the tire, there is no theft problem. In addition, the NFC-based TPMS is cheaper than external Bluetooth-based TPMS devices. Indirect TPMS is not considered in bicycles due to its complexity.

VI. CONCLUSION

The present study has presented the design and measurement of a prototype consisting of a tire pressure sensing tag equipped with NFC technology. A miniaturized tag antenna of 16 × 12 mm has been proposed and its electrical parameters have been measured. The magnetic field received at the tag antenna for different separations between reader and tag has been analyzed. The study has demonstrated the capability of the tag to provide a constant harvested voltage to the circuitry by converting RF to DC, reaching distances of up to 8 mm from the outer part of the tire to the reader keeping at a stable 3 V output. The proposed sensing circuitry is based on a 555 timer in which the frequency of the signal at the output varies according to the value given by a force-sensing resistor that is placed between the tire and the inner tube of a bicycle wheel to sense the pressure. Resolution of 0.1 bar has been achieved in the range 0.5 to 2.2 bar. The microcontroller calculates the pressure using the frequency of the signal that comes from the 555 and the result is stored on the IC tag to be retrieved as plain text by any NFC-enabled device, without the need of any external application. The prototype could also be used to measure the pressure of other objects, such as balls. Several improvements could be made on the prototype in a future path towards commercialization. In order to further minimize the risk of puncturing the tire due to the tag, the device can be manufactured with a flexible substrate. Furthermore, it is possible to reduce the size of the device by integrating the FSR into the PCB.

REFERENCES

[1] S. Walden. *Banking After COVID-19: The Rise of Contactless Payments in the U.S.* Accessed: Mar. 2021. https://www.forbes.com/advisor/banking/banking-after-covid-19-the-rise-%of-contactless-payments-in-the-u-s/

[2] *NFC Forum*. Accessed: Mar. 2021. [Online]. Available: https://nfc-forum.org/

[3] G. Madlmayr, C. Kantner, and T. Grechenig, "Near field communication," in *Secure Smart Embedded Devices, Platforms and Applications*. New York, NY, USA: Springer, 2014, pp. 351–367.

[4] A. Lazaro, M. Boada, R. Villarino, and D. Girbau, "Battery-less smart diaper based on NFC technology," *IEEE Sensors J.*, vol. 19, no. 22, pp. 10848–10858, Nov. 2019.

[5] M. Alabdulhafith, R. V. Sampangi, and S. Sampalli, "NFC-enabled smartphone application for drug interaction and drug allergy detection," in *Proc. 5th Int. Workshop Near Field Commun. (NFC)*, Feb. 2013, pp. 1–6.

[6] N. Anabtawi, S. Freeman, and R. Ferzli, "A fully implantable, NFC enabled, continuous interstitial glucose monitor," in *Proc. IEEE-EMBS Int. Conf. Biomed. Health Informat. (BHI)*, Feb. 2016, pp. 612–615.

[7] J. P. Puma, M. Huerta, R. Alvizu, and R. Clotet, "Mobile identification: NFC in the healthcare sector," in *Proc. 6th Andean Region Int. Conf.*, Nov. 2012, pp. 39–42.

[8] J. Fontecha, R. Hervas, J. Bravo, and V. Villarreal, "An NFC approach for nursing care training," in *Proc. 3rd Int. Workshop Near Field Commun.*, Feb. 2011, pp. 38–43.

[9] H. Kostinger, M. Gobber, T. Grechenig, B. Tappeiner, and W. Schramm, "Developing a NFC based patient identification and ward round system for mobile devices using the Android platform," in *Proc. IEEE Point Care Healthcare Technol. (PHT)*, Jan. 2013, pp. 176–179.

[10] M. Boada, A. Lazaro, R. Villarino, and D. Girbau, "Battery-less NFC sensor for pH monitoring," *IEEE Access*, vol. 7, pp. 33226–33239, 2019.

[11] M. Boada, A. Lázaro, R. Villarino, and D. Girbau, "Battery-less soil moisture measurement system based on a NFC device with energy harvesting capability," *IEEE Sensors J.*, vol. 18, no. 13, pp. 5541–5549, Jul. 2018.

[12] I. L. Ruiz and M. Gómez-Nieto, "University smart poster: Study of NFC technology applications for university ambient," in *Proc. 3rd Symp. Ubiquitous Comput. Ambient Intell.* Berlin, Germany: Springer, 2009, pp. 112–116.

[13] K. Boes, L. Borde, and R. Egger, "The acceptance of NFC smart posters in tourism," in *Information and Communication Technologies in Tourism*. Cham, Switzerland: Springer, 2015, pp. 435–447.

[14] M. V. Bueno-Delgado, P. Pavón-Marino, A. De-Gea-García, and A. Dolón-García, "The smart university experience: An NFC-based ubiquitous environment," in *Proc. 6th Int. Conf. Innov. Mobile Internet Services Ubiquitous Comput.*, Jul. 2012, pp. 799–804.

[15] R. Hardy, E. Rukzio, P. Holleis, G. Broll, and M. Wagner, "MyState: Using NFC to share social and contextual information in a quick and personalized way," in *Proc. 12th ACM Int. Conf. Adjunct Papers Ubiquitous Comput. (Ubicomp)*, 2010, pp. 447–448.

[16] A. Fressancourt, C. Herault, and E. Ptak, "NFCSocial: Social networking in mobility through IMS and NFC," in *Proc. 1st Int. Workshop Near Field Commun.*, Feb. 2009, pp. 24–29.

[17] L. Mainetti, L. Patrono, and R. Vergallo, "IDA-pay: A secure and efficient micro-payment system based on peer-to-peer NFC technology for Android mobile devices," *J. Commun. Softw. Syst.*, vol. 8, no. 4, pp. 117–125, 2012.

[18] P. Pourghomi, M. Qasim, and G. Ghinea, "A proposed NFC payment application," *Int. J. Adv. Comput. Sci. Appl.*, vol. 4, no. 8, pp. 173–181, 2013. [Online]. Available: http://thesai.org/Publications/ViewPaper?Volume=4&Issue=8&Code=IJACSA&SerialNo=24

[19] F. Carré, J. Caudeville, R. Bonnard, V. Bert, P. Boucard, and M. Ramel, "Soil contamination and human health: A major challenge for global soil security," in *Global Soil Security*. Cham, Switzerland: Springer, 2017, pp. 275–295.

[20] K. M. Winslow, S. J. Laux, and T. G. Townsend, "A review on the growing concern and potential management strategies of waste lithium-ion batteries," *Resour., Conservation Recycling*, vol. 129, pp. 263–277, Feb. 2018.

[21] S. Priya and D. Inman, *Energy Harvesting Technologies*, vol. 21. Boston, MA, USA: Springer, 2009.

[22] H. Ryu, H. Yoon, and S. Kim, "Hybrid energy harvesters: Toward sustainable energy harvesting," *Adv. Mater.*, vol. 31, no. 34, Aug. 2019, Art. no. 1802898.

[23] S. Yun, Y. Zhang, Q. Xu, J. Liu, and Y. Qin, "Recent advance in new-generation integrated devices for energy harvesting and storage," *Nano Energy*, vol. 60, pp. 600–619, Jun. 2019.

[24] A. Lazaro, R. Villarino, and D. Girbau, "A survey of NFC sensors based on energy harvesting for IoT applications," *Sensors*, vol. 18, no. 11, p. 3746, Nov. 2018.

[25] A. Lazaro, M. Boada, R. Villarino, and D. Girbau, "Study on the reading of energy-harvested implanted NFC tags using mobile phones," *IEEE Access*, vol. 8, pp. 2200–2221, 2020.

[26] A. Lazaro, M. Boada, R. Villarino, and D. Girbau, "NFC sensors based on energy harvesting for IoT applications," in *Recent Wireless Power Transfer Technologies*, P. Pinho, Ed. Rijeka, Croatia: IntechOpen, 2020, ch. 2, doi: 10.5772/intechopen.89283.

[27] F. Di Rienzo, A. Virdis, C. Vallati, N. Carbonaro, and A. Tognetti, "Evaluation of NFC-enabled devices for heterogeneous wearable biomedical application," *IEEE J. Radio Freq. Identificat.*, vol. 4, no. 4, pp. 373–383, Dec. 2020.

[28] P. Escobedo, M. Bhattacharjee, F. Nikbakhtnasrabadi, and R. Dahiya, "Smart bandage with wireless strain and temperature sensors and batteryless NFC tag," *IEEE Internet Things J.*, vol. 8, no. 6, pp. 5093–5100, Mar. 2021.

[29] S. M. Ali and W.-Y. Chung, "Monitoring transepidermal water loss and skin wettedness factor with battery-free NFC sensor," *Sensors*, vol. 20, no. 19, p. 5549, Sep. 2020.

[30] P. Teengam, W. Siangproh, S. Tontisirin, A. Jiraseree-amornkun, N. Chuaypen, P. Tangkijvanich, C. S. Henry, N. Ngamrojanavanich, and O. Chailapakul, "NFC-enabling smartphone-based portable amperometric immunosensor for hepatitis B virus detection," *Sens. Actuators B, Chem.*, vol. 326, Jan. 2021, Art. no. 128825.

[31] *MLX91804 Product Flyer*. Accessed: Jun. 2021. [Online]. Available: https://www.melexis.com/en/contact/request-product-flyer-tpms

[32] *FXTH87 Family Evaluation Design Reference Manual*. Accessed: Jun. 2021. [Online]. Available: https://www.nxp.com/docs/en/reference-manual/FXTH87EDRM.pdf

[33] A. Bernhard. *The Great Bicycle Boom of 2020*. Accessed: Mar. 2021. [Online]. Available: https://www.bbc.com/future/bespoke/made-on-earth/the-great-bicycle-boom%-of-2020.html

[34] S. Butler. *Cycling Boom Rolls on Amid Struggle to Meet UK Demand During COVID*. Accessed: Mar. 2021. [Online]. Available: https://www.theguardian.com/business/2021/mar/21/cycling-boom-rolls-on-%amid-struggle-to-meet-uk-demand-during-covid

[35] *Wireless Tire Pressure Monitor*. Accessed: Jun. 2021. [Online]. Available: https://sykik.com/collections/wireless-tire-pressure-monitor

[36] *FOBO Bike 2 User Manual Version 1.6*. Accessed: Jun. 2021. [Online]. Available: https://my-fobo.com/manual/FOBO_Bike_2_usermanualversn_1.6.pdf

[37] *ZUMO 590 Owner's Manual*. Accessed: Jun. 2021. [Online]. Available: https://www8.garmin.com/manuals/webhelp/zumo590/EN-US/GUID-63C67DBE-1C1C-4887-A705-FE7B842C5BE9-homepage

[38] C. Kollegger, P. Greiner, C. Steffan, M. Wiessflecker, H. Froehlich, T. Kautzsch, G. Holweg, and B. Deutschmann, "A system-on-chip NFC bicycle tire pressure measurement system," in *Proc. IEEE 60th Int. Midwest Symp. Circuits Syst. (MWSCAS)*, Aug. 2017, pp. 60–63.

[39] S. I. Yaniger, "Force sensing resistors: A review of the technology," in *Proc. Electro Int.*, Apr. 1991, pp. 666–668.

[40] A. Hollinger and M. M. Wanderley, "Evaluation of commercial force-sensing resistors," in *Proc. Int. Conf. New Interfaces Musical Expression*, Paris, France: Citeseer, 2006, pp. 4–8.

[41] D. V. Knudson and S. C. White, "Forces on the hand in the tennis forehand drive: Application of force sensing resistors," *Int. J. Sport Biomech.*, vol. 5, no. 3, pp. 324–331, Aug. 1989.

[42] A. Nikonovas, A. J. L. Harrison, S. Hoult, and D. Sammut, "The application of force-sensing resistor sensors for measuring forces developed by the human hand," *Proc. Inst. Mech. Eng. H, J. Eng. Med.*, vol. 218, no. 2, pp. 121–126, Feb. 2004.

[43] N. K. Rana, "Application of force sensing resistor (FSR) in design of pressure scanning system for plantar pressure measurement," in *Proc. 2nd Int. Conf. Comput. Electr. Eng.*, Dec. 2009, pp. 678–685.

[44] M. Marshall and M. Wanderley, "A survey of sensor use in digital musical instruments," Sound Process. Control Lab., McGill Univ., Montreal, QC, Canada, Tech. Rep., 2004.

[45] G. Ogris, M. Kreil, and P. Lukowicz, "Using FSR based muscule activity monitoring to recognize manipulative arm gestures," in *Proc. 11th IEEE Int. Symp. Wearable Comput.*, Oct. 2007, pp. 45–48.

[46] L. Paredes-Madrid, J. Fonseca, A. Matute, E. Gutiérrez Velásquez, and C. Palacio, "Self-compensated driving circuit for reducing drift and hysteresis in force sensing resistors," *Electronics*, vol. 7, no. 8, p. 146, Aug. 2018.

[47] A. Matute, L. Paredes-Madrid, E. Gutierrez, and C. A. P. Vargas, "Characterization of drift and hysteresis errors in force sensing resistors considering their piezocapacitive effect," in *Proc. IEEE Sensors*, Oct. 2017, pp. 1–3.

[48] A. Matute, L. Paredes-Madrid, G. Moreno, F. Cárdenas, and C. A. Palacio, "A novel and inexpensive approach for force sensing based on FSR piezocapacitance aimed at hysteresis error reduction," *J. Sensors*, vol. 2018, pp. 1–16, Jan. 2018.

[49] J. A. Florez and A. Velasquez, "Calibration of force sensing resistors (fsr) for static and dynamic applications," in *Proc. IEEE ANDESCON*, Sep. 2010, pp. 2–7.

[50] S. Milici, J. Lorenzo, A. Lázaro, R. Villarino, and D. Girbau, "Wireless breathing sensor based on wearable modulated frequency selective surface," *IEEE Sensors J.*, vol. 17, no. 5, pp. 1285–1292, Mar. 2017.

[51] S. Barrett and D. Pack, "Atmel AVR microcontroller primer: Programming and interfacing," *Synth. Lectures Digit. Circuits Syst.*, vol. 7, no. 2, pp. 1–244, 2012.

[52] *NFC Data Exchange Format (NDEF)*, NFC Forum, Wakefield, MA, USA, 2006.

[53] T. Igoe, D. Coleman, and B. Jepson, *Beginning NFC: Near Field Communication With Arduino, Android, and Phonegap*. Sebastopol, CA, USA: O'Reilly Media, 2014.

[54] I. Ortego, N. Sanchez, J. Garcia, F. Casado, D. Valderas, and J. I. Sancho, "Inkjet printed planar coil antenna analysis for NFC technology applications," *Int. J. Antennas Propag.*, vol. 2012, pp. 1–6, Jan. 2012.

[55] M. Gebhart, "Analytical considerations for an ISO/IEC14443 compliant SmartCard transponder," in *Proc. 11th Int. Conf. Telecommun.*, Jun. 2011, pp. 9–16.

[56] M. Ishii and K. Komiyama, "A measurement method for the antenna factor of small loop antenna by measuring the input impedance," in *Proc. Conf. Precis. Electromagn. Meas.*, Jun. 2004, pp. 80–81.
[57] C. Kolle, W. Scherr, D. Hammerschmidt, G. Pichler, M. Motz, B. Schaffer, B. Forster, and U. Ausserlechner, "Ultra low-power monolithically integrated capacitive pressure sensor for tire pressure monitoring," in *Proc. IEEE Sensors*, Oct. 2004, pp. 244–247.
[58] J. Qian, D.-S. Kim, and D.-W. Lee, "On-vehicle triboelectric nanogenerator enabled self-powered sensor for tire pressure monitoring," *Nano Energy*, vol. 49, pp. 126–136, Jul. 2018.
[59] F. Khameneifar and S. Arzanpour, "Energy harvesting from pneumatic tires using piezoelectric transducers," in *Smart Materials, Adaptive Structures and Intelligent Systems*, vol. 43314. London, U.K.: Hindawi, 2008, pp. 331–337.
[60] J. Lee and B. Choi, "Development of a piezoelectric energy harvesting system for implementing wireless sensors on the tires," *Energy Convers. Manage.*, vol. 78, pp. 32–38, Feb. 2014.
[61] J. Lee, J. Oh, H. Kim, and B. Choi, "Strain-based piezoelectric energy harvesting for wireless sensor systems in a tire," *J. Intell. Mater. Syst. Struct.*, vol. 26, no. 11, pp. 1404–1416, Jul. 2015.
[62] C. R. Bowen and M. H. Arafa, "Energy harvesting technologies for tire pressure monitoring systems," *Adv. Energy Mater.*, vol. 5, no. 7, Apr. 2015, Art. no. 1401787.
[63] J. Zhu, L. Wu, X. Zhang, C. Jia, and C. Zhang, "A low-power 433MHz transmitter for battery-less tire pressure monitoring system," in *Proc. 9th IEEE Int. Conf. ASIC*, Oct. 2011, pp. 184–187.
[64] Q. Kang, L. Wu, H. Jiang, and X. Zhang, "An improved 433MHz low power transmitter for batteryless tire pressure monitor system," in *Proc. 12th IEEE Int. Conf. Solid-State Integr. Circuit Technol. (ICSICT)*, Oct. 2014, pp. 1–3.
[65] B. Dixon, V. Kalinin, J. Beckley, and R. Lohr, "A second generation in-car tire pressure monitoring system based on wireless passive SAW sensors," in *Proc. IEEE Int. Freq. Control Symp. Expo.*, Jun. 2006, pp. 374–380.
[66] L. M. Silalahi, M. Alaydrus, A. D. Rochendi, and M. Muhtar, "Design of tire pressure monitoring system using a pressure sensor base," *Sinergi*, vol. 23, no. 1, pp. 70–78, 2019.

MARTI BOADA received the B.Sc. degree (Hons.) in telecommunications engineering from Universitat Rovira i Virgili (URV), Tarragona, Spain, in 2012, the M.Sc. degree in telecommunications engineering and management from the Universitat Politècnica de Catalunya (UPC), Barcelona, Spain, in 2014, and the Ph.D. degree in telecommunications engineering from URV, in 2020.

Since 2020, he has been working as a Postdoctoral Researcher with the Department of Electronic Engineering, URV. His research interests include microwave devices and systems, with an emphasis on RFID, NFC, and wireless sensors.

ANTONIO LAZARO (Senior Member, IEEE) was born in Lleida, Spain, in 1971. He received the master's degree (Hons.) and the Ph.D. degree in telecommunication engineering from the Universitat Politècnica de Catalunya (UPC), Barcelona, Spain, in 1994 and 1998, respectively. He became a Faculty Member of the UPC, where he currently teaches a course on microwave circuits and antennas. Since July 2004, he has been a full-time Professor with the Department of Electronic Engineering, Universitat Rovira i Virgili (URV), Tarragona, Spain. His research interests include microwave device modeling, on-wafer noise measurements, monolithic microwave integrated circuits (MMICs), low-phase noise oscillators, MEMS, RFID, UWB, and microwave systems.

RAMON VILLARINO received the degree (Hons.) in telecommunications technical engineering from Ramon Llull University (URL), Barcelona, Spain, in 1994, and the degree in senior telecommunications engineering and the Ph.D. degree from the Universitat Politècnica de Catalunya (UPC), Barcelona, in 2000 and 2004, respectively. From 2005 to 2006, he was a Research Associate with the Technological Telecommunications Center of Catalonia (CTTC), Barcelona. He worked as a Researcher and an Assistant Professor with the Universitat Autònoma de Barcelona (UAB), from 2006 to 2008. Since January 2009, he has been a full-time Professor with Universitat Rovira i Virgili (URV), Tarragona, Spain. His research interests include radiometry, microwave devices, systems based on UWB, RFIDs, and frequency selective structures using metamaterials (MM).

ERNEST GIL-DOLCET was born in Reus, Spain, in 1965. He received the B.S. degree in electronic engineering from the Universitat de Barcelona, and the Ph.D. degree in industrial computing engineering from the Universitat Politècnica de Catalunya (UPC), Barcelona, Spain, in 1998 and 2001, respectively. Since 2008, he has been a full-time Professor with the Department of Electronic Engineering, Universitat Rovira i Virgili (URV), Tarragona, Spain, where he currently teaches a course on industrial computing. Since 2002, he has been the Director of the URV's CITEE Center, where he has conducted several research and development projects mainly focused on distributed control systems for companies in the industrial, automobile, and railway sectors. His research interests include communication protocols and communication system design.

DAVID GIRBAU (Senior Member, IEEE) received the B.Sc. degree (Hons.) in telecommunication engineering, the master's degree in electronics engineering, and the Ph.D. degree in telecommunication from the Universitat Politècnica de Catalunya (UPC), Barcelona, Spain, in 1998, 2002, and 2006, respectively. From February 2001 to September 2007, he was a Research Assistant with UPC. From September 2005 to September 2007, he was a part-time Assistant Professor with the Universitat Autònoma de Barcelona (UAB). Since October 2007, he has been a full-time Professor with Universitat Rovira i Virgili (URV), Tarragona, Spain. His research interests include microwave devices and systems, with an emphasis on UWB, RFIDs, RF-MEMS, and wireless sensors.